Feed Forward Loop Improves the Transient Dynamics of an Antithetic Biological Controller

Thales R. Spartalis[1], Mathias Foo[2,*], Xun Tang[1,*]

[1] Cain Department of Chemical Engineering, Louisiana State University, Baton Rouge, LA 70803

[2] School of Engineering, University of Warwick, Coventry CV4 7AL, UK.

*Corresponding authors

ABSTRACT

Integral controller is widely used in industry for its capability of endowing perfect adaptation to disturbances. To harness such capability for precise gene expression regulation, synthetic biologists have endeavored in building biomolecular (quasi-)integral controllers, such as the antithetic integral controller. Despite demonstrated successes, challenges remain with designing the controller for improved transient dynamics and adaptation. Here we explore and investigate the design principles of alternative RNA-based biological controllers, by modifying an antithetic integral controller with prevalently found natural feedforward loops, to improve its transient dynamics and adaptation performance. With model-based analysis, we demonstrate that while the base antithetic controller shows excellent responsiveness and adaptation to system disturbances, incorporating the type-1 incoherent feedforward loop into the base antithetic controller could attenuate the transient dynamics caused by changes in the stimuli, especially in mitigating the undesired overshoot in the output gene expression. Further analysis on the kinetic parameters reveals similar findings to previous studies that the degradation and transcription rates of the circuit RNA species would dominate in shaping the performance of the controllers.

KEYWORDS: antithetic controller, feedforward loop; computational analysis; gene circuits

INTRODUCTION

Building synthetic feedback control gene circuits for precise and robust regulation of a gene expression is a longstanding interest to synthetic biologists,[1–7] as it is critical to achieving precise chemical and biological signals mediation, and protein production in coping with internal and external disturbances and unwarranted changes.[8–10] Natural systems provide numerous examples of robust perfect adaptation, including *E. coli* chemotaxis and calcium homeostasis in mammalian cells.[11] In a feedback control scheme, the controller monitors the dynamics of the species of interest to determine the corresponding regulation of the process, and to mitigate or eliminate the impact of disturbances and uncertainties, for improved control precision and robustness. Since synthetic systems often exhibit vulnerabilities to fluctuations in the surrounding environment, the design and implementation of a robust controller are thus essential. This has led to a variety of work on designing and implementing synthetic feedback controllers for cell population regulation, biofuel production, and single cell gene expression regulation.[12–16]

Previous studies demonstrated that the feedback mechanism in a biological system can be achieved with molecular sequestration, using proteins, such as transcription factors, or nucleic acids, such as RNA and antisense RNA.[17–20] Among different feedback controllers, integral controllers are of special interest, as they promise perfect adaptation theoretically. In Briat et. al, an antithetic integral controller is introduced,[5] which employs a sequestration reaction between two controller species, where one actuates the system dynamics and the other is influenced by the system output, to achieve an integral controller design for reference tracking and disturbance adaptation.[2] This mechanism enables the circuit to adapt by showcasing its potential for reference tracking and perfect adaptation to environmental disturbances. [2,5,6,8,9,21] Similar studies include Shopera et al., which presented a negative feedback based transcription controller to adapt for ribosome fluctuation; [22] Agrawal et al., which leveraged σ_{28} and anti-σ_{28} for molecular sequestration

to realize an integral controller; [23] Samaniego et al., [24] which deployed an activation-deactivation reaction cycle and a molecular sequestration to realize an ultrasensitive quasi-integral controller; as well as related works from the Del Vecchio's group. [25–28] However, despite the prosperity of studies on feedback controllers, there still exist limitations to overcome for enhanced reliability and practical implementations. For example, as demonstrated by Refs [6,9,21], the transient dynamics of the antithetic controller need to be further improved for a rapid response to stimuli, and the perfect adaptation requires delicate tuning of the kinetic parameters.[8] Besides, understanding the dynamics of the biological system is also critical to designing effective biological controllers. Therefore, vast research efforts exist where multi-omics kinetic models are used to investigate the dynamic behavior of the biological systems.[29, 30,31] In Ref [32], the authors integrated multiple omics data sources and developed a multi-omics model to predict the genome-wide concentrations and growth dynamics in *E. coli* cells. By incorporating multiple omics layers and known gene regulatory and protein-protein interactions, the model improves the prediction accuracy, providing a broadly applicable framework for guiding biological discovery.[32] In a recent study,[33] Di Filippo et al. developed a computational pipeline which leverages a constraint-based model to integrate metabolomics and transcriptomics data and to characterize multi-level metabolic regulation, considering both enzyme expression levels and metabolites interactions.[33] Finally, a modification to antithetic controllers with additional regulations is proposed in Ref [34], where a biomolecular Proportional-Integral-Derivative controller was proposed to improve the stability of genetic circuits and mitigate stochastic noise in yeast cells. Nevertheless, exploring alternative designs and further understanding the design principles of biological controllers remain an ongoing task.

Designing new biological controllers can be achieved with computational approaches, where given an objective function of the circuit dynamics, one can perform optimization to design the number of nodes (gene elements, such as plasmid, mRNA, and protein) and the interactions, by minimizing the difference between the circuit output and the objective dynamics.[35,36] Alternatively, it can also be achieved with reasoning based on domain expertise, known dynamics and functions of existing regulatory parts and network motifs.[18,37–39] One of the most well-studied network motifs is the feedforward loop (FFL), which is composed of three biological nodes, X, Y, and Z, as shown in Figure 1a. In the Type-1 coherent feedforward loop (CFFL), both X and Y would activate the expression of node Z, whereas, in the Type-1 incoherent feedforward loop (IFFL), X activates Z expression, but Y represses Z expression. The CFFLs and IFFLs are prevalent in the transcriptional networks of bacterial cells.[40–42] For example, Mangan et al. [43] presented the design of CFFL and IFFL circuits with natural motifs, using gene *fnr* and gene *arcA* as the X and Y species, respectively, while realizing a type-1 CFFL with gene *focA* as species Z, or a type-1 IFFL with gene *glpACB* as species Z. Given such prevalence in the biological systems, as well as their well characterized properties and proven functions as signal amplifiers,[43,44] noise filters,[45] fold-change detector,[46] perceptron,[47] and pulse generation,[48–50] here in this study, we investigate the modification of a classical antithetic integral controller proposed in Briat et. al.,[5] with the FFLs, in improving the transient dynamics of the controller and attenuating the impact from disturbances.

Specifically, we conduct a simulation-based analysis of alternative designs of the antithetic controllers. We first analyze their characteristics with widely used parameter values in literature[5,6] without considering their biological feasibility, expecting to grasp a general understanding of each design. To complement the efforts, we then analyze the circuits with kinetic parameters previously fitted to experiments from previous works[51–55] to infer their practical applicability and limitations. The results indicate that proper incorporation of FFL motifs into the base antithetic controller could improve the adaptation and attenuate undesirable overshoot subject to disturbances.

RESULTS AND DISCUSSION

Circuits Design and Mathematical Modeling

We first set off to define a base antithetic controller (hereinafter termed a Base Circuit) as depicted in Figure 1b), as a benchmark to gauge the performance of our proposed circuits. This Base Circuit is composed of nodes A, B, and C, where A and C are independent gene species, and B represents the biological system to be regulated. While B could contain a complex network as shown in the figure, for simplicity, here we consider a single gene expression process in B, for all the circuits introduced in this work. Note that, as we restrict our focus to RNA-based gene circuits, all the gene species described in the work refer to (m)RNA, unless otherwise specified. The production of Gene A is activated by inducer μ, which then promotes gene B production at a transcription rate α_A. Gene B promotes the transcription of gene C at a transcription rate α_B. Genes A and C sequester each other at a sequestration rate of γ_{AC}, to form a feedback function. All genes degrade at their corresponding degradation rate δ. The detailed mechanistic Ordinary Differential Equation (ODE) model is given in Eqn. (1).

$$\begin{aligned}
\frac{d[A]}{dt} &= \mu - \gamma_{AC} \,.\, [A] \,.\, [C] \; - \; \delta_A \,.\, [A] \\
\frac{d[B]}{dt} &= \alpha_A \,.\, [A] - \; \delta_B \,.\, [B] \\
\frac{d[C]}{dt} &= \alpha_B \,.\, [B] \; - \; \gamma_{AC} \,.\, [A] \,.\, [C] - \; \delta_C \,.\, [C]
\end{aligned} \tag{1}$$

We then explore antithetic controllers modified with Type-1 CFFL and Type-1 IFFL motifs. The Type-1 CFFL is widely considered a sign-sensitive delay element, which means it shows a delay only for positive steps, thus acknowledged as an asymmetric filter. [18] The Type-1 IFFL circuit is well recognized as a pulse generator, offering speed increase to dynamic responses of the system.[50] Therefore, we expect the incorporation of the Type-1 CFFL and IFFL motifs would benefit the transient dynamics of the Base Circuit, such as accelerated response to the stimuli, rapid settling after the disturbance, and moderate overshoot if there is any. Note that, while the number of the FFL motifs and the locations for them to be integrated into the Base Circuit would contribute to numerous architectures, we have confined our design up to two motifs in the circuit, to avoid overly complex designs. Based on our preliminary investigation (Figures S1 to S3), three designs showed the best performances in terms of both transient and steady state dynamics.

Specifically, the first FFL- modified circuit is the CFFL-based antithetic controller, as shown in Eqn. (2), and is named CFFL-based Circuit throughout the rest of this manuscript. In comparison to the Base Model, one CFFL motif is introduced to establish a promotion pathway from gene C to gene A, where gene C directly promotes the transcription of gene X in the CFFL motif, and the CFFL motif output gene Z promotes the transcription of gene A. Such a design amplifies the sensitivity of gene A to changes in gene C, thus holding the promise of accelerating and strengthening the feedback response from the sequestration reaction. Within the CFFL, we assumed the same activation rate α from gene X to genes Y and Z, for simplicity, but we expect a customized activation/transcription rate for each species to deliver further improved dynamics for specific applications. On the other hand, all genes degrade at their corresponding degradation rate δ. The detailed ODE model of this circuit is shown in Eqn. (2).

$$\begin{aligned}
\frac{d[A]}{dt} &= \mu + \alpha_Z . [Z] - \; \gamma_{AC} \,.\, [A] \,.\, [C] \; - \; \delta_A \,.\, [A] \\
\frac{d[B]}{dt} &= \alpha_A \,.\, [A] - \; \delta_B \,.\, [B] \\
\frac{d[X]}{dt} &= \alpha_C \,.\, [C] - \; \delta_X \,.\, [X] \\
\frac{d[Y]}{dt} &= \alpha_X \,.\, [X] - \; \delta_Y \,.\, [Y]
\end{aligned}$$

$$\frac{d[Z]}{dt} = \alpha_X . [X] + \alpha_Y . [Y] - \delta_Z . [Z]$$
$$\frac{d[C]}{dt} = \alpha_B . [B] - \gamma_{AC} . [A] . [C] - \delta_C . [C] \quad (2)$$

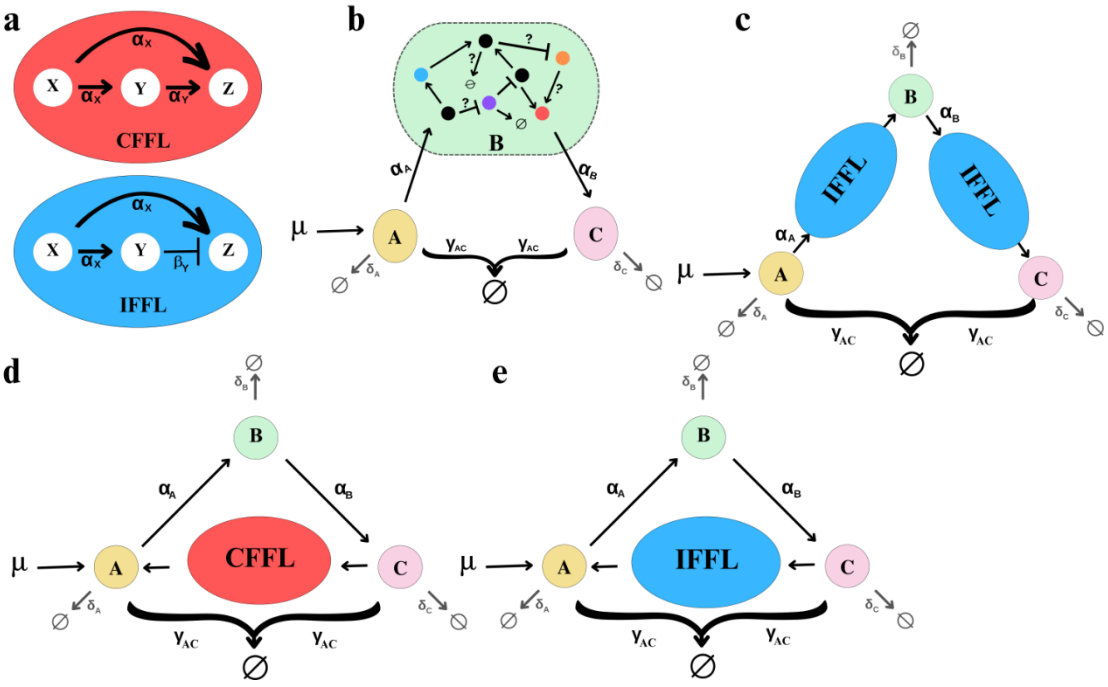

Figure 1. Schematics of different antithetic controller designs. a) CFFL and IFFL are composed of three nodes X, Y, and Z. b) Base Circuit with B representing a single gene expression process. c) CFFL-based Circuit. d) 1IFFL-based Circuit. e) 2IFFL-based Circuit.

Two IFFL-modified circuits stood out among all the tested designs in this study. The first one features one IFFL circuit between genes C and A, to form an activation pathway from gene C to gene A as shown in Figure 1d) and is named as 1IFFL-based Circuit. This design seems to share the same intention as in the CFFL-based Circuit to enhance the interaction between genes A and C. The second IFFL-based circuit features two IFFL circuits, named as 2IFFL-based Circuit, with one in the gene A to gene B activation pathway, and the other in the gene B to gene C activation pathway. Different from the 1IFFL-based Circuit, the 2IFFL-based Circuit seems to emphasize on accelerating the response of genes B and C in affecting the overall dynamics of the circuit. The detailed ODE models for these two designs are given in Eqn. (3) and (4), respectively. Note, in the 2IFFL-based Circuit, "X1" and "X2" refers to the X species in the IFFL between A and B, and the IFFL between B and C respectively. The same applies to genes Y and Z.

$$\frac{d[A]}{dt} = \mu + \alpha_Z . [Z] - \gamma_{AC} . [A] . [C] - \delta_A . [A]$$
$$\frac{d[B]}{dt} = \alpha_A . [A] - \delta_B . [B]$$

$$\frac{d[X]}{dt} = \alpha_C . [C] - \delta_X . [X]$$
$$\frac{d[Y]}{dt} = \alpha_X . [X] - \beta_Y . [Z][Y] - \delta_Y . [Y]$$
$$\frac{d[Z]}{dt} = \alpha_X . [X] - \beta_Y . [Z][Y] - \delta_Z . [Z]$$
$$\frac{d[C]}{dt} = \alpha_B . [B] - \gamma_{AC} . [A] . [C] - \delta_C . [C] \quad (3)$$

$$\frac{d[A]}{dt} = \mu + \alpha_Z . [Z] - \gamma_{AC} . [A] . [C] - \delta_A . [A]$$
$$\frac{d[B]}{dt} = \alpha_Z . [Z1] - \delta_B . [B]$$
$$\frac{d[X1]}{dt} = \alpha_A . [A] - \delta_X . [X1]$$
$$\frac{d[Y1]}{dt} = \alpha_X . [X1] - \beta_Y . [Y1][Z1] - \delta_Y . [Y1]$$
$$\frac{d[Z1]}{dt} = \alpha_X . [X1] - \beta_Y . [Y1][Z1] - \delta_Z . [Z1]$$
$$\frac{d[C]}{dt} = \alpha_Z . [Z2] - \gamma_{AC} . [A] . [C] - \delta_C . [C]$$
$$\frac{d[X2]}{dt} = \alpha_B . [B] - \delta_X . [X2]$$
$$\frac{d[Y2]}{dt} = \alpha_X . [X2] - \beta_Y . [Y2][Z2] - \delta_Y . [Y2]$$
$$\frac{d[Z2]}{dt} = \alpha_X . [X2] - \beta_Y . [Y2][Z2] - \delta_Z . [Z2] \quad (4)$$

For experimental realization, the FFL motifs can be constructed with RNA-regulators such as STAR, and toehold switches,[56–58] and the sequestration between species A and C can be designed with antisense RNAs.[19,59] The engineered FFL motifs can then be integrated into the system to be controlled by incorporating at least one identified gene, expressing either a fluorescent protein (GFP) or proteins quantifiable via SDS-PAGE.[60,61]

Controller Performance Evaluation

The dynamics of a gene circuit can be affected by the kinetic parameters associated with the embedded reactions, as they could fluctuate in a real system due to changes in cellular resources and environmental disturbances, such as the transcription and the degradation rates (i.e. α and δ in our ODE models). For example, the availability of polymerase would affect the transcription rate, and ambient temperature could also affect the transcription rate of heat-sensitive promoters. Therefore, here we quantify the circuit response subject to parameter perturbations. Furthermore, we consider two sets of nominal parameter values: 1) a generic set of parameters, which does not necessarily bear biological relevance but have been widely adopted in mathematical analysis of gene circuits dynamics.[6,21,62] With this effort, we aim to complement existing analysis from a different perspective on antithetic controllers, and more importantly to gain an assessment of the circuit properties with less constricted requirements on the kinetic parameters, given the possibility that novel regulatory parts would emerge to make it feasible to realize currently

seemingly unfeasible parameter values. 2) a set of parameters obtained from fitting to experiments in previous studies.[63,64] With this effort, we thrive to evaluate the characteristics of these circuits for potential practical application, given existing synthetic gene regulatory tools.

To analyze the performance of the circuits, we introduced a step change in the inducer concentration at time zero and adopted the same four standard step-change response analysis metrics from our previous work:[39] *rise time*, which quantifies the responsiveness of the system to a change in the environment; *overshoot*, which measures the difference between the maximum of a system's response to changes in the environment from its final steady-state value (if a steady state is to be achieved) during the transient period; *settling time*, which characterizes the speed at which a system settles after the disturbance; and *relative steady state error*, which quantifies the capability of tracking the reference at steady state (if a steady state is to be achieved). We anticipate the four metrics to capture both transient and steady state behaviors of the system, with rise time and settling time to provide a measure of the dynamic response of the system to environmental changes, and the overshoot together with steady state error to shed light on the adaptation and robustness of the system. To evaluate their capability of disturbance adaptation, we also perturbed the output concentration with a step change after the system reached steady state) and quantified the steady state error before and after the perturbance, as well as the settling time as defined above. For illustration purpose, results for perturbation of a 10% increase in the output concentration are presented in the main manuscript, while results for higher perturbances (50% and 100%) included in the Supplemental Material, which aim to evaluate the robustness of each circuit.

Circuit Performance with Generic Kinetic Parameters

We first examined the dynamics of the controllers by varying the transcription and degradation rates of the non-FFL species within 0.1 to 10 times the nominal parameter values given in Table S1, a range consistent to previous works, [2,5,6] whereas inducer $\mu = 100\, Mh^{-1}$, gene B activation rate $\alpha_B = 10\, h^{-1}$, and sequestration rate $\gamma_{AC} = 1 \times 10^3\, M^{-1}h^{-1}$, were kept constant. This design of analysis is based on previous findings that the activation and degradation rates dominantly affect the circuit stability.[6] The transcription, repression and degradation rates associated with the FFL circuits were tuned to ensure the system would reach a steady state. The detailed information on the kinetic parameters is provided in Table S1.

As shown in Figure 2, in response to the step change at time zero, the 1IFFL-based Circuit demonstrated the fastest settling to a steady state after around 300 mins, for low transcription and degradation rates (Figure 2a), while the 2IFFL-based Circuit provided the slowest response despite the only one that displayed no oscillatory transient in the output concentration (Figure 2d). The addition of the CFFL motif introduced more oscillatory transient as compared to the Base Circuit, except for low degradation rates cases (Figure 2a, b and c), whereas the IFFL motif tends to reduce the oscillatory transient behavior in the circuit, with the 2IFFL motifs displaying almost no oscillatory transient behavior, albeit at the cost of a slower response to the inducer concentration change. An increase in transcription rate α (from the left to the right plots) lead to an increased responsiveness and steady state gene B expression in the Base Circuit, the CFFL-based Circuit, and the 1IFFL-based Circuit, with an amplified overshoot and oscillatory transient dynamics (Figure 2d-f). However, increasing the transcription rate resulted in similar responsiveness and gene B steady state expression in the 2IFFL-based Circuit, showing robust dynamics to the other three circuits. These opposing behavioral outcomes arise as a result of the positioning and configuration of the FFLs. Even though, placing an IFFL before gene B attenuates the impact of increase in gene A on gene B expression, an additional IFFL placed before gene C offers a compensation of this impact by attenuating gene C expression, which increases the sequestration between gene C and A. Placing an IFFL between gene B and gene C attenuates impact on gene C due to gene B expression increase, as a result, the sequestration between gene C and A would dominate the dynamics that as the transcription rate increases, gene B expression decreases.

While all four circuits demonstrated robustness to variations in transcription rate in terms of adaptation, significant variations in degradation rate (Figure 2g and h) resulted in obvious deviation from the reference.

Interestingly, while increasing the degradation rate leads to decreased expression of gene B, a combination of high transcription and degradation rates leads to a fast and precise adaptation in the Base Circuit, CFFL-based and IFFL-based, while 2IFFL-based presents a precise but slower performance (Figure 2i). This outcome could be attributed to the competition between the IFFL impact on gene B production and the sequestration reaction between genes A and C in the 2IFFL-based Circuit, as gene A concentration would positively correlate to gene B production, but the IFFL between genes A and B tends to attenuate such activation effect.

When subjected to the perturbation introduced, all circuits demonstrated perfect adaptation, in terms of settling to the original steady state before the disturbance. Except for the 2IFFL-based Circuit, all the other three circuits exhibited oscillatory behavior before regaining the steady state, as shown in Figure 2. These observations indicate that adding the IFFL circuits to the base antithetic controller could attenuate the oscillatory behavior and mitigate the impact on the steady state concentration subject to variation in certain kinetic parameters, such as the degradation rate, while the addition of the CFFL circuit would potentially introduce more pronounced oscillations.

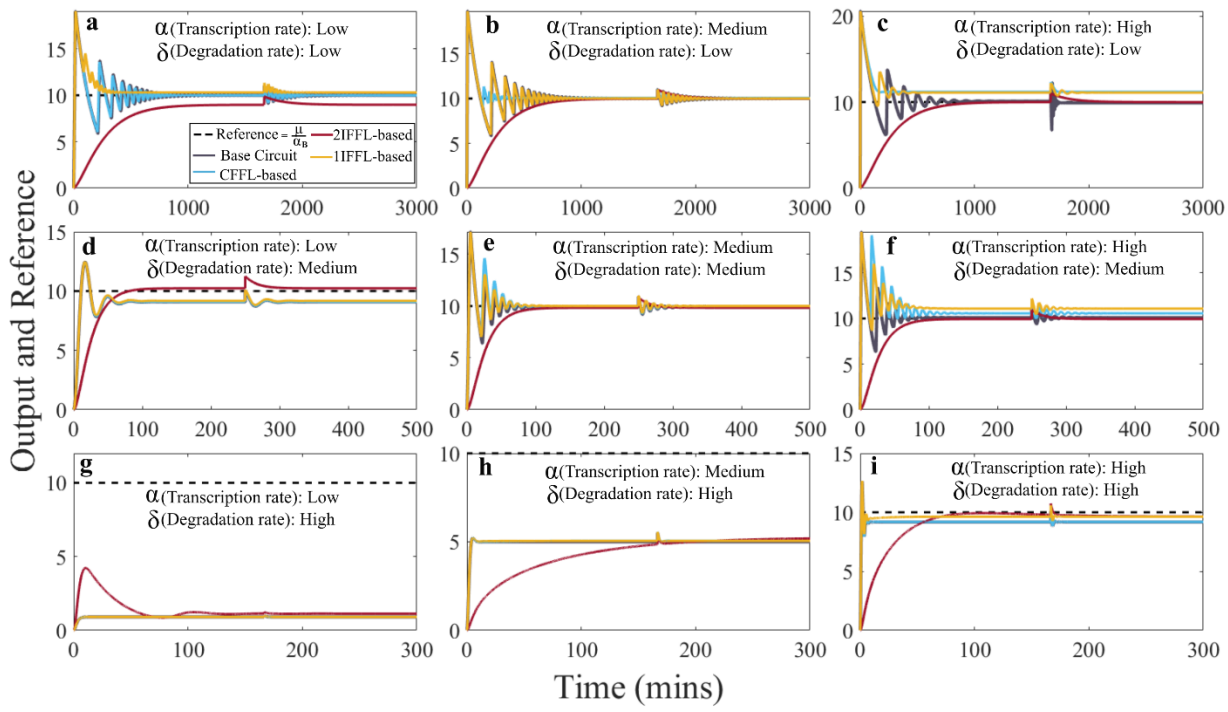

Figure 2. Controller performance to varying transcription and degradation rates, with different scenarios: Scenario Low rate: $\alpha_A = \alpha_C = 1\ h^{-1}$, $\delta_A = \delta_B = \delta_C = 0.1\ h^{-1}$; Medium rate: $\alpha_A = \alpha_C = 10\ h^{-1}$, $\delta_A = \delta_B = \delta_C = 1\ h^{-1}$; High rate: $\alpha_A = \alpha_C = 100\ h^{-1}$, $\delta_A = \delta_B = \delta_C = 10\ h^{-1}$.

Circuit Performance with Experimentally Fitted Kinetic Parameters

While the circuit analysis with parameters that are less confined by biological relevance could provide a more general understanding of its dynamics, such kinetics might not be achievable in experiments given the current development of gene regulatory tools. As the goal of designing synthetic gene circuits is to deliver desired functions in real biological systems, analysis with biologically relevant parameters would become crucial. Therefore, for the subsequent sections, we focus our analysis with kinetic parameters inferred from previously experimentally fitting.[51,63] The detailed information on the kinetic parameters is provided in Table S2.

With parameters from Table S2, the CFFL-based Circuit demonstrated an unstable behavior in gene B expression, where the output gene expression diverges as time increases (see Figure S4). This observation differs significantly from the analysis with the non-biologically feasible parameters, but makes sense given that the non-biologically feasible parameters offer more freedom in parameter design that the specific sets of parameters tested did not capture the unstable dynamics observed here. As the addition of the CFFL motif between genes A and C constructs a competition with the sequestration, depending on the specific kinetics of the sequestration and the CFFL activation pathway, unstable behavior in gene B expression could eventually emerge. Since the CFFL-based Circuit did not yield adaptation, its analysis is not included in the following main text but provided in the Supplemental Material.

As we aim for biological controller designs that delivers excellent transient dynamics as well as reference tracking, but not necessarily (quasi-)integral controllers, we also notice that a previously reported antithetic controller with negative feedback from gene C to gene B (Figure 3) could improve the dynamics in mammalian cells. [9] For completeness, we include this design (named as FB-based Circuit here) in our analysis along with the remaining two IFFL-based circuits. Instead of the Hill-type function modeling considered in Gupta and Khammash, [9] here we develop a simple ODE model given in Eqn. (5), to represent the FB-based Circuit for a consistent comparison with the other circuits.

$$\begin{aligned}
\frac{d[A]}{dt} &= \mu - \gamma_{AC} \,.\, [A] \,.\, [C] \; - \; \delta_A \,.\, [A] \\
\frac{d[B]}{dt} &= \alpha_A \,.\, [A] - \beta_{CB} \,.\, [B] \,.\, [C] - \; \delta_B \,.\, [B] \\
\frac{d[C]}{dt} &= \alpha_B \,.\, [B] \; - \beta_{CB} \,.\, [C] \,.\, [B] - \; \gamma_{AC} \,.\, [A] \,.\, [C] - \; \delta_C \,.\, [C]
\end{aligned} \tag{5}$$

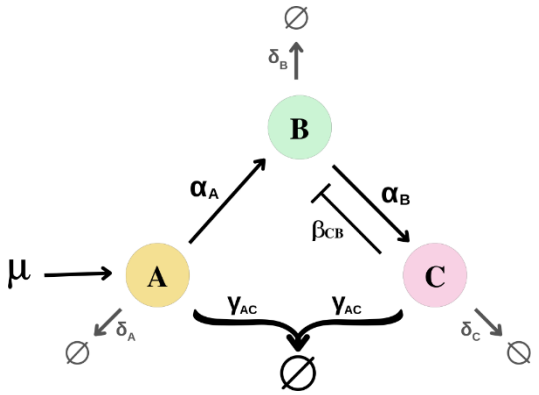

Figure 3. Schematic FB-based Circuit, i.e., the antithetic controller with feedback from gene C to gene B.

Analysis with Varying Transcription and Degradation Rates

To be consistent with the analysis with the generic parameters, we first analyzed the circuit dynamics by varying only the transcription and degradation rates within 0.1 to 10 times the nominal parameter values given in Table S2. The inducer $\mu = 10^{-7}\, Ms^{-1}$, sequestration rate $\gamma_{AC} = 5 \times 10^5\, M^{-1}s^{-1}$, gene B transcription rate $\alpha_B = \; 10^{-1}\, s^{-1}$, and the repression from gene C to gene B, $\beta_{CB} = 10^5 M^{-1}s^{-1}$, were all kept constant. The results are summarized in Figure 4.

Both the Base Circuit (black plots) and the 2IFFL-based Circuit (red plots) showed remarkable adaptation under the tested scenarios, especially when the transcription rate increases, and for the 2IFFL-based Circuit,

the impact of a high transcription rate can be mitigated by a high degradation rate to ensure perfect adaptation (Figure 4i). Moreover, in all the scenarios, the Base Circuit demonstrated a rapid and oscillatory response to the stimuli before settling to the steady state, while the 2IFFL-based Circuit showed no oscillation, but with a slow ramping increase in the gene B expression until reaching the steady state. Surprisingly, the FB-based Circuit (green plots) failed to achieve perfect adaptation in all nine scenarios but demonstrated the fastest response to stimuli change without oscillation. This might be because the feedback interaction is modeled as a consumption between genes B and C here, whereas a Hill type repression function could potentially mitigate the aggressive dynamics [9]. Also contrary to our expectation, the 1IFFL-based Circuit (yellow plots) did not yield adaptation in most scenarios, except for scenarios with low transcription rates combined to medium and high degradation rates (Figure 4d and g), and also demonstrated significant transient oscillatory behavior. To completement the transient dynamics analysis, we also performed equilibrium analysis for each of the circuits, subjecting to different transcription and degradation rates in Supplementary Materials Figure S9. We noticed that the Base Circuit displayed minimal sensitivity to changes in the degradation rate, whereas both the 1IFFL-based and 2IFFL-based circuits demonstrated significant dependence on both the transcription and degradation rates. The detailed results and discussion are provided in the Supplementary Materials document.

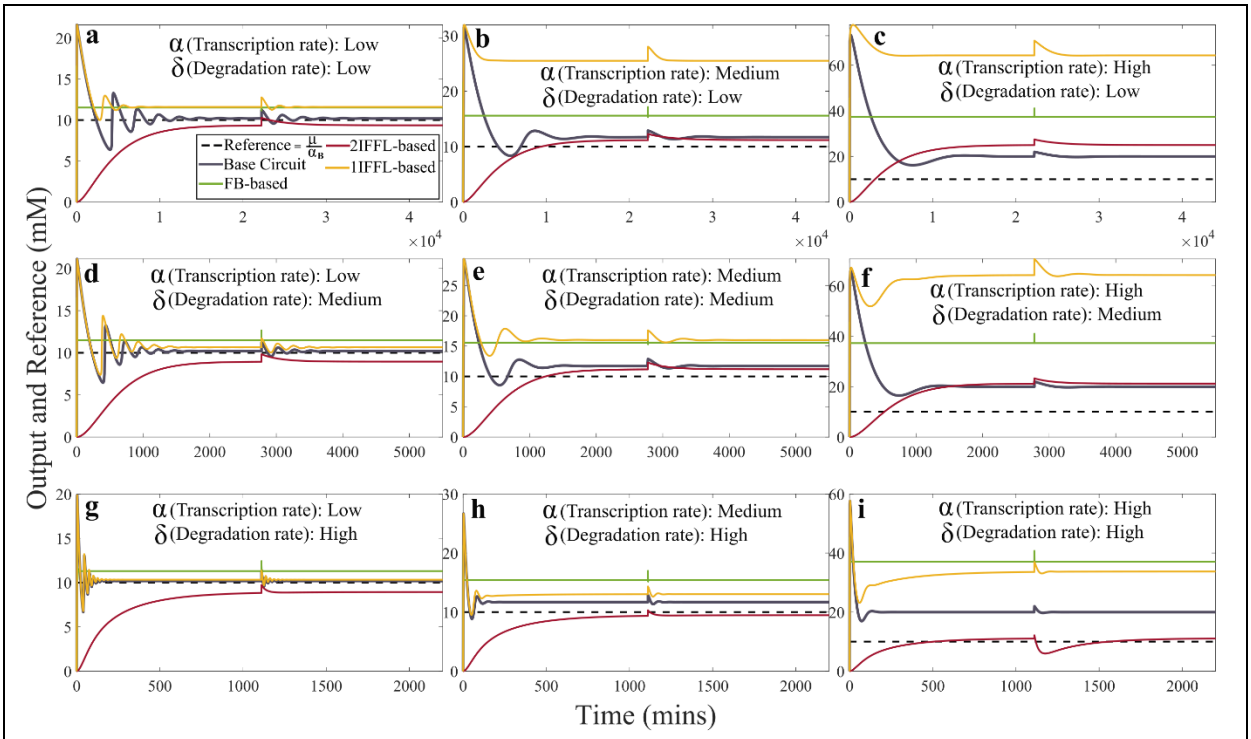

Figure 4. Controller performance to varying transcription and degradation rates, with previous experimentally fitted parameters and: Low rate: $\alpha_A = \alpha_C = 10^{-2}\ s^{-1}$, $\delta_A = \delta_B = \delta_C = 10^{-5}\ s^{-1}$; Medium rate: $\alpha_A = \alpha_C = 10^{-1}\ s^{-1}$, $\delta_A = \delta_B = \delta_C = 10^{-4}\ s^{-1}$; High rate: $\alpha_A = \alpha_C = 1\ s^{-1}$, $\delta_A = \delta_B = \delta_C = 10^{-3}\ s^{-1}$. Inset figure in a) shows the fast transient dynamics of the FB-base Circuit.

Global Sensitivity Analysis for Statistical Analysis

To gain a more statistically significant understanding of the four circuits, we then performed a global sensitivity analysis with 1000 simulations, where all the model kinetic parameters were randomly perturbed within 0.1x and 10x of their corresponding nominal values given in Table S2. For this sensitivity analysis, no perturbation was introduced after the system reached the steady state.

Of the 1000 simulations, 996, 947, 648, and 1000 simulations reached steady state after the initial 2000 minutes, for the Base Circuit, the 1IFFL-based Circuit, the 2IFFL-based Circuit, and the FB-based Circuit, respectively. This observation indicates that both the Base Circuit and the FB-based Circuit are robust to variations in the kinetic parameters, whereas incorporating the IFFL motif could undermine such robustness, in terms of converging to a steady state. This is probably due to the increased complexity in the IFFL-modified circuits. Moving forward, we focused our analysis on these simulations that have reached a steady state for each circuit.

The distributions of overshoot, relative steady state error, settling time, and rise time after the step change at time 0 in Figure 5 demonstrate that: 1) the two IFFL-based Circuits and the FB-based Circuit all endowed a smaller overshoot as compared to the Base Circuit, indicated by the left-skewed distribution of the overshoot in Figure 5a, with the 2IFFL-based Circuit showing the lowest overshoot. 2) the FB-based Circuit demonstrated the best performance in terms of relative steady state error, and both the 1IFFL-based and the FB-based Circuit also showed similarly small relative steady state error. While the 2IFFL-based Circuit also yielded small relative steady state error, it tends to yield a lower than reference steady state value (thus a negative steady state error) rather than a higher than steady state value as observed in the other three circuits. 3) The FB-based Circuit showed the best performance in terms of rapid settling time and fast response to stimuli (rise time) as depicted in Figures 5c and 5d. While the Base Circuit showed a comparable responsiveness to stimuli (rise time) in Figure 5d, the settling time could span from minutes to hundreds of minutes, depending on the specific values of the kinetic parameters as shown in Figure 5c. On the other hand, while the 1IFFL-based Circuit improved the settling time as compared to the Base Circuit, the addition of the IFFL motif resulted in a wide distribution of the settling time as in Figure 5d. This is more prominent with the 2IFFL-based Circuit, where both the rise time and the settling time span from minutes to hundreds of minutes, suggesting a slower dynamic compared to the Base and the FB-based Circuit.

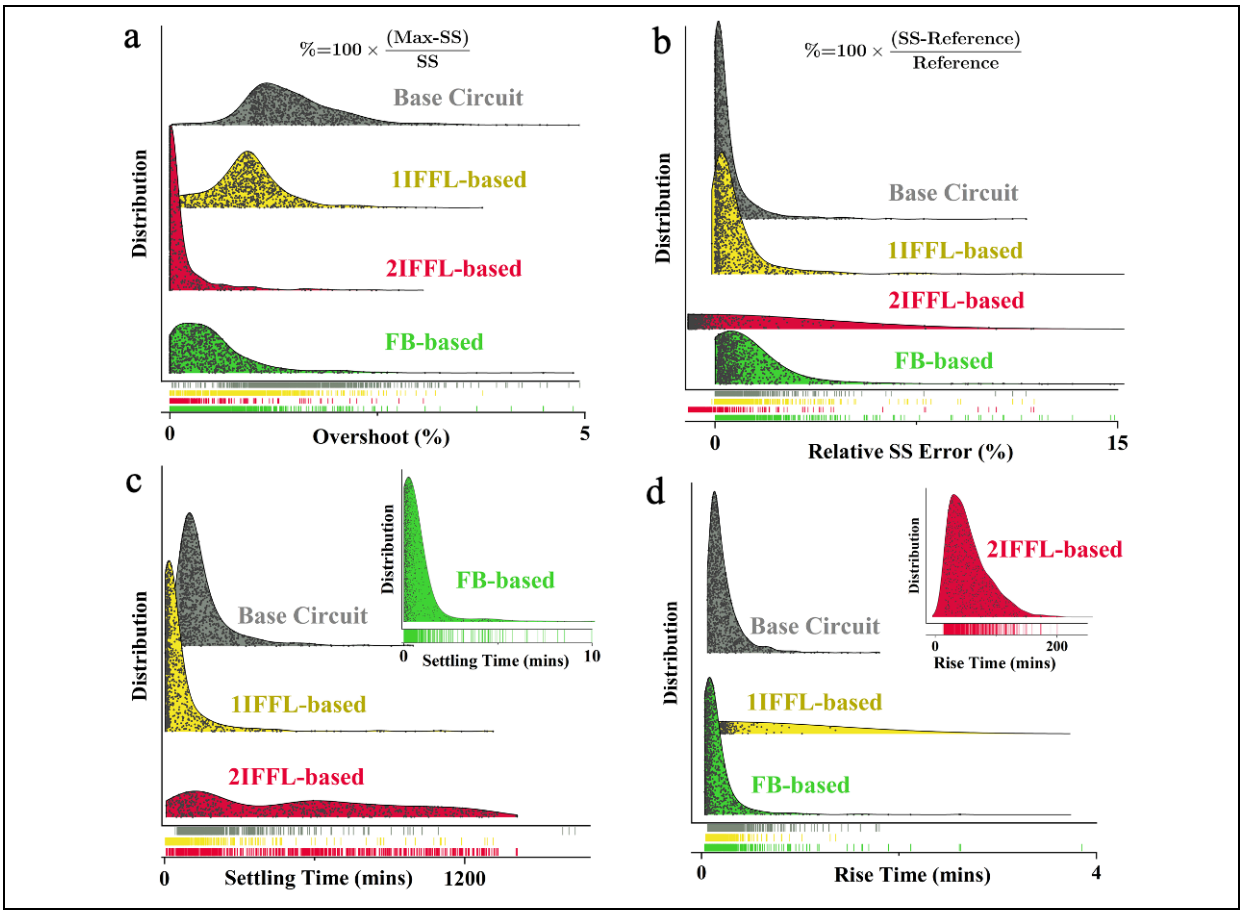

Figure 5. Global sensitivity analysis with simulations reached steady state without a second perturbation, in terms of: a) overshoot; b) relative steady state error; c) settling time; and d) rise time. The dots beneath each plot show the location of all the data on the x-axis.

Further analysis on the kinetic parameter requirements for the two IFFL-based Circuits to achieve a rapid response (rise time $\leq$ 60 mins), moderate overshoot (|overshoot| $\leq$ 1%), fast adaptation (settling time $\leq$ 120 mins), and reasonable relative steady state error (|error| $\leq$ 1%), reveals a higher flexibility in designing the parameters for the 2IFFL-based Circuit, as compared to the 1IFFL-based Circuit. Specifically, as indicated in Figure 6, the 2IFFL-based Circuit (red plot in Figure 6b) would require a high degradation rate for genes B (δ_X) and Z (δ_Z), but a low degradation of gene Y (δ_Y), gene C (δ_C), and B (δ_B), showing no obvious preference in the remaining nine parameters. In contrast, the 1IFFL-based Circuit (yellow plot in Figure 6b) would require a high degradation rate of gene C (δ_C), but a low transcription rate of genes A (α_A) and B (α_B), as well as a relatively higher sequestration rate between genes A and C (γ_{AC}), with no obvious preference in the remaining 11 parameters. It is noteworthy that the parameters employing the most significant influence on the circuit are limited to transcription and degradation rates. This observation aligns with the stability analysis elucidated by Olsman et al.,[6] which asserts that the stability of the antithetic integral type of circuits is dominated by the values of transcription and degradation rates.

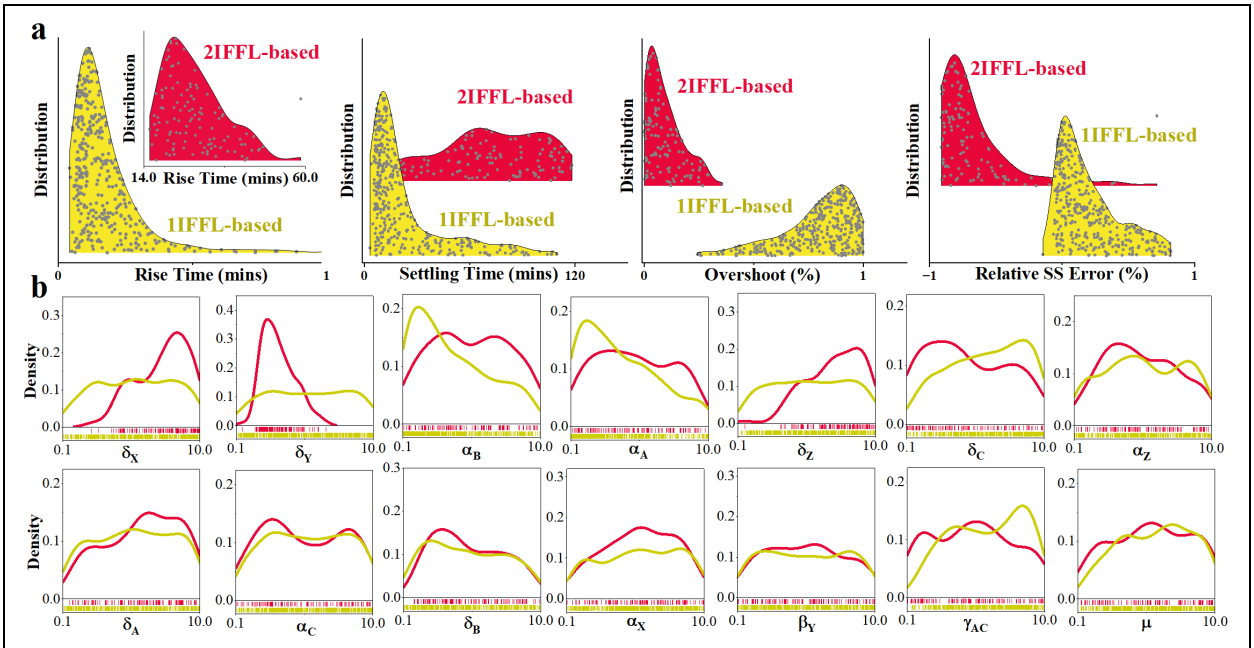

Figure 6. Desired kinetic parameter ranges for antithetic controller with IFFL-based Circuits to deliver a rapid response and settling to changes in inducer stimuli, with mitigated overshoot and adaptation.

We also performed a sensitivity analysis for simulations with secondary perturbation (10%) after reaching the steady state in Figure 7. Result demonstrates that while all four circuits yielded comparable adaptation, the relative percentage steady state error in Figure 7a shows that the FB-based circuit exhibited the fastest settling time, whereas the Base Circuit showed the slowest settling dynamics. This observation indicates that the direct feedback pathway and the addition of IFFL circuits could accelerate the transient dynamics in disturbance adaptation of the Base Circuit.

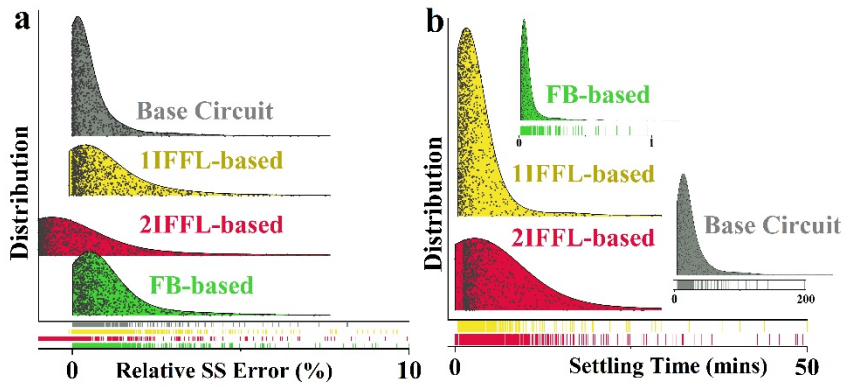

Figure 7. Global sensitivity analysis for simulations after disturbance in terms of: a) Relative Steady-State Error; b) Settling Time. 10% perturbation.

CONCLUSIONS

In this work, we investigated the dynamics of different antithetic controllers modified with the feedforward loop biological motifs and evaluated the benefits and limitations of such modifications through simulation. Our results demonstrate that while the Base Circuit excels in adaptation and rapid stimuli response, its oscillatory dynamics with significant overshoot could have resulted from the disturbances in the inducer. The introduction of a negative feedback to repress the expression of the target gene could contribute to mitigated overshoot with significantly enhanced response to stimuli, demonstrated by the rapid rise time and settling time in the FB-based Circuit. However, such an aggressive interaction could result in compromised adaptation. In contrast, adding the IFFL motif to the Base Circuit could in general effectively attenuate the oscillatory dynamics, and mitigate unwanted overshoot due to changes in the inducer concentration. However, analysis with biologically feasible parameters suggests, circuits modified with the IFFL motif could potentially slow down the response to stimuli changes, and the mitigation and elimination of the oscillation could also result in a slow adaptation to steady state. These phenomena would probably be due to the increased complexity in the design as a result of adding the IFFL motifs to the Base Circuit. To achieve a circuit with a fast response and settling time, as well as a moderate overshoot and mitigated oscillation, a delicate design of the kinetic parameters would be necessary.

Given the prevalence of the IFFL motif in natural biological systems, as well as the development of novel synthetic designs of the IFFL circuits, [65–68] we expect a wider application of the IFFL circuits in more complicated biological regulators for enhanced functionalities. The performance of a synthetic gene circuit in real system implementation is always undermined by cellular resource competition with native biological activities, thus a design with light cellular burden is normally preferred. However, this typically comes at the price of limited functionality. Recent advancement in the division of labor,[69–71] where a complicated circuit is split into parts and implemented in different groups or species of cells to carry out independent activities and communicate via quorum sensing to deliver the anticipated overall function, was found capable of reducing cellular burden and mitigating the impact of resource competition on the performance. We anticipate research efforts in this direction, as well as on leveraging resource competition as a negative control to cooperatively regulate the circuit dynamics, to facilitate the implementation of a complex circuit on real biological systems.

The work presented here offers a computational analysis of different alternative antithetic controllers and serves as a preliminary step towards the design of novel synthetic circuits with advanced functions using existing biological motifs. While analysis with less emphasis on the biological relevance could offer a general understanding of the circuit properties, especially with analytical studies on the architectural properties[2,8,21,72] as the circuit dynamics is significantly affected by the specific kinetic parameter values,

discrepancies could arise when biological relevance is considered. This suggests that for practical applications, analysis centered around biologically feasible conditions is vital in guiding the design and construction of novel circuits. As the circuit dynamics is context-dependent, experimental characterization of basic genetic regulatory parts under different conditions could offer a more reliable range of biological feasible parameter values, to facilitate the simulation-based analysis, and in return, to accelerate the exploration of new circuits with enhance performances. In future research, we plan to validate the proposed IFFL-based antithetic controller in both *E. coli* and cell-free systems, to gauge the performance in experiments, as well as the reliability of model-based analysis. We envision such efforts to further contribute to our understanding on building novel circuits with natural biological regulatory motifs for advanced functionalities, and to the experiment-simulation integrated exploration for new synthetic circuits.

METHODS

Mathematical Models and Simulation

The ODE-based models were constructed for each antithetic controller design and solved utilizing the MATLAB `ode23s` solver. These models accounted for species interactions involving activation, degradation, sequestration, and repression, with kinetic parameters derived from established literature in the field. The sensitivity analysis was executed by systematically altering all kinetic parameters within the model. In each simulation, the designated kinetic parameters for each circuit were multiplied by a "scaling factor," spanning from 10^{-1} to 10. This approach facilitated a thorough exploration of the parameter space, providing insights into the models' sensitivity to variations in kinetic parameters. 1000 simulations were performed for each genetic circuit in the sensitivity analysis, and the violin plots presented in Figure 5 were generated using Origin Pro. All the MATLAB scripts used for simulation in this study can be found at https://github.com/Thales-Spartalis/Code-Feed_Forward_Loop_Improves_the_Transient_Dynamics_of_an_Antithetic_Biological_Controller.

AUTHORS INFORMATION

Corresponding Author

***Email:** xuntang@lsu.edu; M.Foo@warwick.ac.uk

ORCID

Thales R. Spartalis: 0000-0001-6655-5912; Mathias Foo: 0000-0003-1400-2659; Xun Tang: 0000-0003-0317-9176

Author contributions

X.T., M.F. conceptualized the work, X.T., M.F., T.S. developed the model, T.S. performed the simulation and computational analysis, T.S. and X.T. performed results interpretation. All authors contributed to the writing.

Notes

The authors declare no competing financial interest and no conflict of interest.

ACKNOWLEDGMENTS

X.T. and T.R.S. are supported by NSF grant #2223720.

REFERENCES

(1) Briat, C.; Gupta, A.; Khammash, M. Antithetic Proportional-Integral Feedback for Reduced Variance and Improved Control Performance of Stochastic Reaction Networks. *J R Soc Interface* **2018**, *15* (143). https://doi.org/10.1098/rsif.2018.0079.

(2) Baetica, A. A.; Leong, Y. P.; Murray, R. M. Guidelines for Designing the Antithetic Feedback Motif. *Phys Biol* **2020**, *17* (5). https://doi.org/10.1088/1478-3975/ab8454.

(3) Cuba Samaniego, C.; Franco, E. Ultrasensitive Molecular Controllers for Quasi-Integral Feedback. *Cell Syst* **2021**, *12* (3), 272-288.e3. https://doi.org/10.1016/j.cels.2021.01.001.

(4) Boada, Y.; Vignoni, A.; Pico, J. Multiobjective Identification of a Feedback Synthetic Gene Circuit. *IEEE Transactions on Control Systems Technology* **2020**, *28* (1), 208–223. https://doi.org/10.1109/TCST.2018.2885694.

(5) Briat, C.; Gupta, A.; Khammash, M. Antithetic Integral Feedback Ensures Robust Perfect Adaptation in Noisy Bimolecular Networks. *Cell Syst* **2016**, *2* (1), 15–26. https://doi.org/10.1016/j.cels.2016.01.004.

(6) Olsman, N.; Baetica, A. A.; Xiao, F.; Leong, Y. P.; Murray, R. M.; Doyle, J. C. Hard Limits and Performance Tradeoffs in a Class of Antithetic Integral Feedback Networks. *Cell Syst* **2019**, *9* (1), 49-63.e16. https://doi.org/10.1016/j.cels.2019.06.001.

(7) Shannon, B.; Zamora-Chimal, C. G.; Postiglione, L.; Salzano, D.; Grierson, C.; Marucci°, L.; Savery°, N. J.; Di Bernardo°, M. In Vivo Feedback Control of an Antithetic Molecular-Titration Motif in Escherichia Coli Using Microfluidics. *ACS Synth Biol* **2020**, *9* (10), 2617–2624. https://doi.org/10.1101/2020.02.28.952143.

(8) Filo, M.; Khammash, M. Optimal Parameter Tuning of Feedback Controllers with Application to Biomolecular Antithetic Integral Control. In *Proceedings of the IEEE Conference on Decision and Control*; Institute of Electrical and Electronics Engineers Inc., 2019; Vol. 2019-December, pp 951–957. https://doi.org/10.1109/CDC40024.2019.9029430.

(9) Gupta, A.; Khammash, M. An Antithetic Integral Rein Controller for Bio-Molecular Networks. In *Proceedings of the IEEE Conference on Decision and Control*; Institute of Electrical and Electronics Engineers Inc., 2019; Vol. 2019-December, pp 2808–2813. https://doi.org/10.1109/CDC40024.2019.9029864.

(10) Baetica, A.-A.; Westbrook, A.; El-Samad, H. Control Theoretical Concepts for Synthetic and Systems Biology. *Curr Opin Syst Biol* **2019**, *14*, 50–57.

(11) Khammash, M. H. Perfect Adaptation in Biology. *Cell Syst* **2021**, *12* (6), 509–521. https://doi.org/10.1016/j.cels.2021.05.020.

(12) Vera, M.; Biswas, J.; Senecal, A.; Singer, R. H.; Park, H. Y. Single-Cell and Single-Molecule Analysis of Gene Expression Regulation. *Annu Rev Genet* **2016**, *50*, 267–291. https://doi.org/10.1146/annurev-genet-120215-034854.

(13) Liu, W.; Shomron, N. Analysis of MicroRNA Regulation and Gene Expression Variability in Single Cell Data. *J Pers Med* **2022**, *12* (10). https://doi.org/10.3390/jpm12101750.

(14) Siu, Y.; Fenno, J.; Lindle, J. M.; Dunlop, M. J. Design and Selection of a Synthetic Feedback Loop for Optimizing Biofuel Tolerance. *ACS Synth Biol* **2018**, *7* (1), 16–23. https://doi.org/10.1021/acssynbio.7b00260.

(15) Mantzaris, N. V. A Cell Population Balance Model Describing Positive Feedback Loop Expression Dynamics. *Comput Chem Eng* **2005**, *29* (4), 897–909. https://doi.org/10.1016/j.compchemeng.2004.09.012.

(16) Frei, T.; Chang, C.-H.; Filo, M.; Arampatzis, A.; Khammash, M. A Genetic Mammalian Proportional-Integral Feedback Control Circuit for Robust and Precise Gene Regulation. *Proc Natl Acad Sci U S A* **2022**, *119* (24). https://doi.org/10.1073/pnas.

(17) Alon, U. Network Motifs: Theory and Experimental Approaches. *Nat Rev Genet* **2007**, *8* (6), 450–461. https://doi.org/10.1038/nrg2102.

(18) Uri Alon. *An Introduction to Systems Biology: Design Principles of Biological Circuits*, 2nd ed.; CRC Press: Boca Raton, FL, 2020.

(19) Tom, J.; Lu; Aneka; Wu, K. Antisense RNA Insert Design for Plasmid Construction to Knockdown Target Gene Expression. *JEMI methods* **2017**, *1*, 7–15.

(20) Waters, L. S.; Storz, G. Regulatory RNAs in Bacteria. *Cell*. Elsevier B.V. February 20, 2009, pp 615–628. https://doi.org/10.1016/j.cell.2009.01.043.

(21) Filo, M.; Hou, M.; Khammash, M. A Hidden Proportional Feedback Mechanism Underlies Enhanced Dynamic Performance and Noise Rejection in Sensor-Based Antithetic Integral Control. *bioRxiv* **2023**. https://doi.org/10.1101/2023.04.16.537062.

(22) Shopera, T.; He, L.; Oyetunde, T.; Tang, Y. J.; Moon, T. S. Decoupling Resource-Coupled Gene Expression in Living Cells. *ACS Synth Biol* **2017**, *6* (8), 1596–1604. https://doi.org/10.1021/acssynbio.7b00119.

(23) Agrawal, D. K.; Marshall, R.; Noireaux, V.; Sontag, E. D. In Vitro Implementation of Robust Gene Regulation in a Synthetic Biomolecular Integral Controller. *Nat Commun* **2019**, *10* (1). https://doi.org/10.1038/s41467-019-13626-z.

(24) Cuba Samaniego, C.; Franco, E. Ultrasensitive Molecular Controllers for Quasi-Integral Feedback. *Cell Syst* **2021**, *12* (3), 272-288.e3. https://doi.org/10.1016/j.cels.2021.01.001.

(25) Huang, H. H.; Qian, Y.; Del Vecchio, D. A Quasi-Integral Controller for Adaptation of Genetic Modules to Variable Ribosome Demand. *Nat Commun* **2018**, *9* (1). https://doi.org/10.1038/s41467-018-07899-z.

(26) Barajas, C.; Del Vecchio, D. Synthetic Biology by Controller Design. *Curr Opin Biotechnol* **2022**, *78* (102837). https://doi.org/10.1016/j.copbio.2022.102837.

(27) Qian, Y.; Del Vecchio, D. Robustness of Networked Systems to Unintended Interactions with Application to Engineered Genetic Circuits. *IEEE Trans Control Netw Syst* **2021**, *8* (4), 1705–1716. https://doi.org/10.1109/TCNS.2021.3078144.

(28) Del Vecchio, D.; Dy, A. J.; Qian, Y. Control Theory Meets Synthetic Biology. *J R Soc Interface* **2016**, *13* (20160380). https://doi.org/10.1098/rsif.2016.0380.

(29) Dickinson, Q.; Aufschnaiter, A.; Ott, M.; Meyer, J. G. Multi-Omic Integration by Machine Learning (MIMaL). *Bioinformatics* **2022**, *38* (21), 4908–4918. https://doi.org/10.1093/bioinformatics/btac631.

(30) Kastelic, M.; Kopač, D.; Novak, U.; Likozar, B. Dynamic Metabolic Network Modeling of Mammalian Chinese Hamster Ovary (CHO) Cell Cultures with Continuous Phase Kinetics Transitions. *Biochem Eng J* **2019**, *142*, 124–134. https://doi.org/10.1016/j.bej.2018.11.015.

(31) Erklavec Zajec, V.; Novak, U.; Kastelic, M.; Japelj, B.; Lah, L.; Pohar, A.; Likozar, B. Dynamic Multiscale Metabolic Network Modeling of Chinese Hamster Ovary Cell Metabolism Integrating N-Linked Glycosylation in Industrial Biopharmaceutical Manufacturing. *Biotechnol Bioeng* **2021**, *118* (1), 397–411. https://doi.org/10.1002/bit.27578.

(32) Kim, M.; Rai, N.; Zorraquino, V.; Tagkopoulos, I. Multi-Omics Integration Accurately Predicts Cellular State in Unexplored Conditions for Escherichia Coli. *Nat Commun* **2016**, *7*. https://doi.org/10.1038/ncomms13090.

(33) Di Filippo, M.; Pescini, D.; Galuzzi, B. G.; Bonanomi, M.; Gaglio, D.; Mangano, E.; Consolandi, C.; Alberghina, L.; Vanoni, M.; Damiani, C. INTEGRATE: Model-Based Multi-Omics Data Integration to Characterize Multi-Level Metabolic Regulation. *PLoS Comput Biol* **2022**, *18* (2). https://doi.org/10.1371/journal.pcbi.1009337.

(34) Filo, M.; Kumar, S.; Khammash, M. A Hierarchy of Biomolecular Proportional-Integral-Derivative Feedback Controllers for Robust Perfect Adaptation and Dynamic Performance. *Nat Commun* **2022**, *13* (1). https://doi.org/10.1038/s41467-022-29640-7.

(35) Hiscock, T. W. Adapting Machine-Learning Algorithms to Design Gene Circuits. *BMC Bioinformatics* **2019**, *20* (1). https://doi.org/10.1186/s12859-019-2788-3.

(36) Merzbacher, C.; Oyarzún, D. A. Applications of Artificial Intelligence and Machine Learning in Dynamic Pathway Engineering. *Biochemical Society Transactions*. Portland Press Ltd October 1, 2023, pp 1871–1879. https://doi.org/10.1042/BST20221542.

(37) Ogorelova, D.; Sadyrbaev, F. Remarks on the Mathematical Modeling of Gene and Neuronal Networks by Ordinary Differential Equations. *Axioms* **2024**, *13* (61). https://doi.org/10.3390/axioms13010061.

(38) Vághy, M. A.; Otero-Muras, I.; Pájaro, M.; Szederkényi, G. A Kinetic Finite Volume Discretization of the Multidimensional PIDE Model for Gene Regulatory Networks. *Bull Math Biol* **2024**, *86* (2). https://doi.org/10.1007/s11538-023-01251-3.

(39) Smolen, P.; Baxter, D. A.; Byrne, J. H. Modeling Transcriptional Control in Gene Networks - Methods, Recent Results, and Future Directions. *Bull Math Biol* **2000**, *62* (2), 247–292. https://doi.org/10.1006/bulm.1999.0155.

(40) Ma, W.; Trusina, A.; El-Samad, H.; Lim, W. A.; Tang, C. Defining Network Topologies That Can Achieve Biochemical Adaptation. *Cell* **2009**, *138* (4), 760–773. https://doi.org/10.1016/j.cell.2009.06.013.

(41) Shen-Orr, S. S.; Milo, R.; Mangan, S.; Alon, U. Network Motifs in the Transcriptional Regulation Network of Escherichia Coli. *Nat Genet* **2002**, *31* (1), 64–68. https://doi.org/10.1038/ng881.

(42) Milo, R.; Shen-Orr, S.; Itzkovitz, S.; Kashtan, N.; Chklovskii, D.; Alon, U. Network Motifs: Simple Building Blocks of Complex Networks. *Science (1979)* **2002**, *298*, 824–827.

(43) Mangan, S.; Alon, U. Structure and Function of the Feed-Forward Loop Network Motif. *Proc Natl Acad Sci U S A* **2003**, *100* (21), 11980–11985.

(44) Pieters, P. A.; Nathalia, B. L.; Van Der Linden, A. J.; Yin, P.; Kim, J.; Huck, W. T. S.; De Greef, T. F. A. Cell-Free Characterization of Coherent Feed-Forward Loop-Based Synthetic Genetic Circuits. *ACS Synth Biol* **2021**, *10* (6), 1406–1416. https://doi.org/10.1021/acssynbio.1c00024.

(45) Chakravarty, S.; Csikász-Nagy, A. Systematic Analysis of Noise Reduction Properties of Coupled and Isolated Feedforward Loops. *PLoS Comput Biol* **2021**, *17* (12). https://doi.org/10.1371/JOURNAL.PCBI.1009622.

(46) Litovco, P.; Barger, N.; Li, X.; Daniel, R. Topologies of Synthetic Gene Circuit for Optimal Fold Change Activation. *Nucleic Acids Res* **2021**, *49* (9), 5393–5406. https://doi.org/10.1093/nar/gkab253.

(47) Rizik, L.; Danial, L.; Habib, M.; Weiss, R.; Daniel, R. Synthetic Neuromorphic Computing in Living Cells. *Nat Commun* **2022**, *13* (1). https://doi.org/10.1038/s41467-022-33288-8.

(48) Ryan, J.; Hong, S.; Foo, M.; Kim, J.; Tang, X. Model-Based Investigation of the Relationship between Regulation Level and Pulse Property of I1-FFL Gene Circuits. *ACS Synth Biol* **2022**, *11* (7), 2417–2428. https://doi.org/10.1021/acssynbio.2c00109.

(49) Zong, D. M.; Sadeghpour, M.; Molinari, S.; Alnahhas, R. N.; Hirning, A. J.; Giannitsis, C.; Ott, W.; Josić, K.; Bennett, M. R. Tunable Dynamics in a Multistrain Transcriptional Pulse Generator. *ACS Synth Biol* **2023**, *12* (12), 3531–3543. https://doi.org/10.1021/acssynbio.3c00434.

(50) Weldemichael, T.; Asemoloye, M. D.; Marchisio, M. A. Feedforward Loops: Evolutionary Conserved Network Motifs Redesigned for Synthetic Biology Applications. *Applied Sciences* **2022**, *12* (8292). https://doi.org/10.3390/app12168292.

(51) Ryan, J.; Hong, S.; Foo, M.; Kim, J.; Tang, X. Model-Based Investigation of the Relationship between Regulation Level and Pulse Property of I1-FFL Gene Circuits. *ACS Synth Biol* **2022**, *11* (7), 2417–2428. https://doi.org/10.1021/acssynbio.2c00109.

(52) Hong, S.; Jeong, D.; Ryan, J.; Foo, M.; Tang, X.; Kim, J. Design and Evaluation of Synthetic Rna-Based Incoherent Feed-Forward Loop Circuits. *Biomolecules* **2021**, *11* (8). https://doi.org/10.3390/biom11081182.

(53) Westbrook, A.; Tang, X.; Marshall, R.; Maxwell, C. S.; Chappell, J.; Agrawal, D. K.; Dunlop, M. J.; Noireaux, V.; Beisel, C. L.; Lucks, J.; Franco, E. Distinct Timescales of RNA Regulators Enable the Construction of a Genetic Pulse Generator. *Biotechnol Bioeng* **2019**, *116* (5), 1139–1151. https://doi.org/10.1002/bit.26918.

(54) Green, A. A.; Silver, P. A.; Collins, J. J.; Yin, P. Toehold Switches: De-Novo-Designed Regulators of Gene Expression. *Cell* **2014**, *159* (4), 925–939. https://doi.org/10.1016/j.cell.2014.10.002.

(55) Chappell, J.; Watters, K. E.; Takahashi, M. K.; Lucks, J. B. A Renaissance in RNA Synthetic Biology: New Mechanisms, Applications and Tools for the Future. *Curr Opin Chem Biol* **2015**, *28*, 47–56. https://doi.org/10.1016/j.cbpa.2015.05.018.

(56) Chappell, J.; Takahashi, M. K.; Lucks, J. B. Creating Small Transcription Activating RNAs. *Nat Chem Biol* **2015**, *11* (3), 214–220. https://doi.org/10.1038/nchembio.1737.

(57) Green, A. A.; Silver, P. A.; Collins, J. J.; Yin, P. Toehold Switches: De-Novo-Designed Regulators of Gene Expression. *Cell* **2014**, *159* (4), 925–939. https://doi.org/10.1016/j.cell.2014.10.002.

(58) Waters, L. S.; Storz, G. Regulatory RNAs in Bacteria. *Cell* **2009**, *136*, 615–628. https://doi.org/10.1016/j.cell.2009.01.043.

(59) Sczakiel, G. The Design of Antisense RNA. *Antisense Nucleic Acid Drug Dev* **1997**, *7*, 439–444.

(60) Albano, C. R.; Randers-Eichhorn, L.; Bentley, W. E.; Rao, G. Green Fluorescent Protein as a Real Time Quantitative Reporter of Heterologous Protein Production. *Biotechnol Prog* **1998**, *14* (2), 351–354. https://doi.org/10.1021/bp970121b.

(61) Alba, F. J.; Daban, J. R. Rapid Fluorescent Monitoring of Total Protein Patterns on Sodium Dodecyl Sulfate-Polyacrylamide Gels and Western Blots before Immunodetection and Sequencing. *Electrophoresis* **1998**, *19* (14), 2407–2411. https://doi.org/10.1002/elps.1150191408.

(62) Zand, A. M.; Tavazoei, M. S. Synthetic Biology-Inspired Robust-Perfect-Adaptation-Achieving Control Systems: Model Reduction and Stability Analysis. *IEEE Trans Control Netw Syst* **2021**, *8* (1), 233–245. https://doi.org/10.1109/TCNS.2020.3038835.

(63) Hu, C. Y.; Varner, J. D.; Lucks, J. B. Generating Effective Models and Parameters for RNA Genetic Circuits. *ACS Synth Biol* **2015**, *4* (8), 914–926. https://doi.org/10.1021/acssynbio.5b00077.

(64) Ryan, J.; Hong, S.; Foo, M.; Kim, J.; Tang, X. Model-Based Investigation of the Relationship between Regulation Level and Pulse Property of I1-FFL Gene Circuits. *ACS Synth Biol* **2022**, *11* (7), 2417–2428. https://doi.org/10.1021/acssynbio.2c00109.

(65) Cournac, A.; Sepulchre, J. A. Simple Molecular Networks That Respond Optimally to Time-Periodic Stimulation. *BMC Syst Biol* **2009**, *3*. https://doi.org/10.1186/1752-0509-3-29.

(66) Frei, T.; Cella, F.; Tedeschi, F.; Gutiérrez, J.; Stan, G. B.; Khammash, M.; Siciliano, V. Characterization and Mitigation of Gene Expression Burden in Mammalian Cells. *Nat Commun* **2020**, *11* (1). https://doi.org/10.1038/s41467-020-18392-x.

(67) Shi, W.; Ma, W.; Xiong, L.; Zhang, M.; Tang, C. Adaptation with Transcriptional Regulation. *Sci Rep* **2017**, *7*. https://doi.org/10.1038/srep42648.

(68) Segall-Shapiro, T. H.; Sontag, E. D.; Voigt, C. A. Engineered Promoters Enable Constant Gene Expression at Any Copy Number in Bacteria. *Nat Biotechnol* **2018**, *36* (4), 352–358. https://doi.org/10.1038/nbt.4111.

(69) Zong, D. M.; Sadeghpour, M.; Molinari, S.; Alnahhas, R. N.; Hirning, A. J.; Giannitsis, C.; Ott, W.; Josić, K.; Bennett, M. R. Tunable Dynamics in a Multistrain Transcriptional Pulse Generator. *ACS Synth Biol* **2023**, *12* (12), 3531–3543. https://doi.org/10.1021/acssynbio.3c00434.

(70) Martinelli, V.; Salzano, D.; Fiore, D.; Di Bernardo, M. Multicellular PI Control for Gene Regulation in Microbial Consortia. *IEEE Control Syst Lett* **2022**, *6*, 3373–3378. https://doi.org/10.1109/LCSYS.2022.3184922.

(71) Fiore, D.; Salzano, D.; Cristòbal-Cóppulo, E.; Olm, J. M.; Di Bernardo, M. Multicellular Feedback Control of a Genetic Toggle-Switch in Microbial Consortia. *IEEE Control Syst Lett* **2021**, *5* (1), 151–156. https://doi.org/10.1109/LCSYS.2020.3000954.

(72) Anastassov, S.; Filo, M.; Chang, C. H.; Khammash, M. A Cybergenetic Framework for Engineering Intein-Mediated Integral Feedback Control Systems. *Nat Commun* **2023**, *14* (1). https://doi.org/10.1038/s41467-023-36863-9.